Enhanced photoluminescence extraction efficiency from a diamond photonic crystal via leaky modes

New Journal of Physics
The open-access journal for physics

Enhanced photoluminescence extraction efficiency from a diamond photonic crystal via leaky modes

L Ondič[1,2,3,6], K Kůsová[1], O Cibulka[1], I Pelant[1], K Dohnalová[1,4], B Rezek[1], O Babchenko[1], A Kromka[1] and N Ganesh[5,7]

[1] Institute of Physics, Academy of Sciences of the Czech Republic, v.v.i., Cukrovarnická 10, CZ-162 53, Prague 6, Czech Republic
[2] Faculty of Mathematics and Physics, Charles University, Ke Karlovu 3, 121 16 Prague 2, Czech Republic
[3] IPCMS–DON Unité Mixte, UMR 7504, CNRS–ULP, 23 rue du Loess, BP 43, 67034 Strasbourg Cedex 2, France
[4] Van der Waals–Zeeman Institute, University of Amsterdam, Valckenierstraat 65, NL-1018 XE Amsterdam, The Netherlands
[5] Nano Sensors Group, University of Illinois at Urbana-Champaign, Champaign, IL, USA
E-mail: ondic@fzu.cz

New Journal of Physics **13** (2011) 063005 (13pp)
Received 26 January 2011
Published 1 June 2011
Online at http://www.njp.org/
doi:10.1088/1367-2630/13/6/063005

Abstract. Two-dimensional photonic crystal can be exploited as the top part of a light source in order to increase its extraction efficiency. Here, we report on the room-temperature intrinsic photoluminescence (PL) behavior of a nanocrystalline diamond (NCD) layer with diamond columns prepared on the top and periodically ordered into the lattice with square symmetry. Angle-resolved far-field measurements in the Γ–X crystal direction of broadband visible PL revealed up to six-fold enhancement of extraction efficiency as compared to a smooth NCD layer. A photonic band diagram above the lightcone derived from these measurements is in agreement with the diagram obtained from transmission measurements and simulation, suggesting that the enhancement is primarily due to light's coupling to leaky modes.

[6] Author to whom any correspondence should be addressed.
[7] Current address: Intel Corporation, 2501 NW 229th Street, Hillsboro, OR, USA.

Contents

1. Introduction

Diamond is a material that possesses very good physical and chemical properties (such as extreme hardness, high thermal conductivity, high electric breakdown field, negative electron affinity and chemical inertness [1–3]). Owing to its wide energy bandgap (5.47 eV), diamond is promising for optoelectronic applications, raising the possibility of, for example, the preparation of ultraviolet (UV) light-emitting diodes (LEDs) [4, 5]. Moreover, under green external illumination, diamond exhibits relatively strong photoluminescence (PL) in the red region of the visible spectrum due to nitrogen-vacancy (N-V) defect centers with short excited-state lifetimes of the order of ns [6]. Apart from the N-V centers, which are studied the most, many other defects (color centers) [1] can be excited by UV irradiation and made to emit light in the red, green or blue spectral region. Therefore, diamond, if pumped electrically, could also be used as a 'white' LED. The main obstacle seems to be a high refractive index of diamond in the visible spectrum, strongly limiting the light extraction efficiency due to a high total internal reflection. Several methods of increasing an LED's light extraction efficiency are available: for example, flip-chip LEDs [7], thin-film rough-surface LEDs [8] or photonic crystal (PhC) LEDs (see the review on PhC LEDs in [9, 10]). The last group can be divided into the following two categories.

1. *Strongly coupled PhC*. The PhC structure penetrates the entire device and its photonic bandgap is tuned so that it spectrally overlaps with the emission spectrum of the light source, which leads to an enhancement of extraction efficiency of LEDs; this type of PhC was theoretically studied by, e.g., Fan *et al* [11] and experimentally by Fujita *et al* [12].
2. *Weakly coupled PhC*. A two-dimensional (2D) PhC etched only at the top of the waveguiding layer is used as a diffraction grating that allows outcoupling of the guided modes from the layer [13, 14]. Moreover, the angular pattern of the emission can be controlled by tuning the characteristics of the PhC.

We will now focus our attention on the latter, the weakly coupled PhC. Usually, an electrically pumped quantum well with a relatively narrow emission spectrum is used as a light source inside the photonic structure and the dimensions/properties of the PhC are chosen to fit the

emitted spectrum in order to increase the extraction efficiency of such a spectrally narrow source [13–15]. In the present case of a spectrally wide emission spectrum of diamond nanocrystals, we aimed to calculate the properties of the PhC in order to efficiently extract a wide range of wavelengths from the structure, in contrast to the usual narrow spectral line extraction. In addition, the spectrally broad PL emission of nanocrystalline diamond (NCD) can be used to study the effect of the PhC over a broad spectral region.

One of the experimental methods used for the characterization of the PhC effect on the luminescence of an integrated light source is an angularly and spectrally resolved far-field radiation measurement [10, 16]. It reveals how the extraction efficiency of luminescence from a sample with the PhC differs from that without it. Moreover, the photonic band diagram (dispersion relations) within the lightcone of free photons[8], which corresponds to modes that are extended to the air surrounding the waveguide, can be extracted from the far-field radiation pattern.

Another commonly used experimental technique that can reveal the PhC band diagram inside the lightcone is the measurement of the transmitivity or reflectivity of the sample. In this case, the incident plane wave of a given frequency, polarization and incidence angle is coupled to the structure only if both the energy and in-plane wavevector match the PhC dispersions. Transmission or reflection spectra obtained from the PhC show resonant features superimposed on the Fabry–Pérot (F–P) background [17–19].

In this paper, we apply both the above-described experimental methods to a 2D PhC with a square lattice symmetry prepared at the top of an NCD layer, in order to study the PhC effect on the intrinsic PL characteristics of diamond. Combination of these methods allows the identification of modes lying in the air lightcone whose character is in agreement with a simple model of band folding of uncorrugated waveguide dispersions. These results considerably extend our previous work on the enhancement of light extraction from an NCD layer with PhC [20], and they allow us to show directly that the increase in extraction efficiency from an NCD layer is mainly due to light's coupling to leaky modes.

2. Experimental

2.1. Preparation of the sample

2.1.1. Nanocrystalline diamond (NCD) layer. An NCD layer was grown on a quartz substrate by plasma-enhanced chemical vapor deposition (PECVD). Here we will give only a brief description of this process; the details can be found in [21]. First, a cleaned quartz substrate with surface area of $10 \times 10\,\mathrm{mm}^2$ was ultrasonically treated in a suspension of ultradispersed diamond powder for ∼40 min. Then, the NCD layer was grown by PECVD (microwave power 1.4 kW, 1% methane in hydrogen, total gas pressure 30 mbar and substrate temperature 560 °C). No additional nitrogen doping was applied during this process. The final thickness of the NCD film was estimated to be ∼417 nm by optical transmission measurements. A typical PL spectrum of these layers covers the whole visible region [22].

2.1.2. Photonic crystal (PhC) grating. PhC structure, prepared at the top of the NCD layer, consists of periodically ordered diamond nanopillars with a square lattice symmetry.

[8] An air lightcone is defined as a region of light frequencies $\omega > c|\mathbf{k}_\parallel|$, where $\mathbf{k}_\parallel$ is an in-plane wavevector.

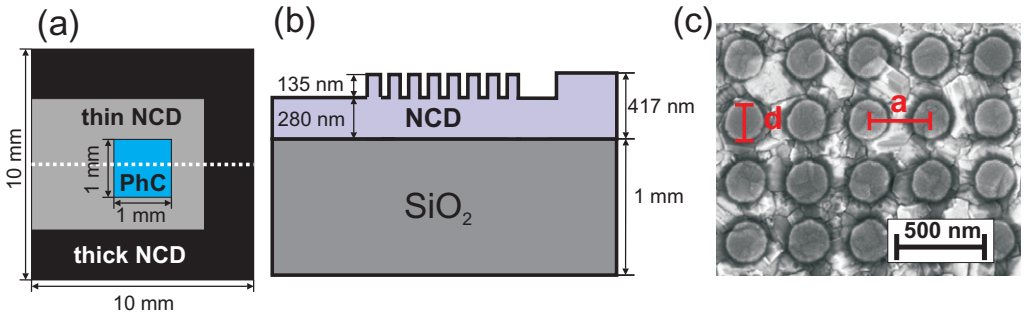

Figure 1. (a) Overall dimensional sketch of the sample, with a square PhC structure located in the middle (top view). (b) Cross-section of the sample along the white dotted line depicted in (a). (c) Top view SEM image of a part of the PhC pillar structure.

Characteristic dimensions were chosen in order to achieve effective extraction of optical guided modes within the whole NCD emission spectrum, based on suggestions given in [9, 23]. The PhC preparation process involved the following steps. The NCD films were coated with an electron-sensitive polymer, which was nanopatterned by electron beam lithography (EBL) using the e-LiNE system (Raith GmbH). The base matrix consisted of regularly repeated holes with a diameter of 250 nm ordered into a square lattice with a lattice constant of $a \sim 350$ nm. Then, a masking matrix was formed by evaporating a nickel layer on the polymer followed by the lift-off strategy. The plasma etching that followed led to the formation of geometrically ordered nanopillars having a height of 135 ± 15 nm (measured by AFM, not shown here) and a diameter of $d \sim 220$ nm (figure 1(c)—as measured by SEM). The PhC structure with a surface area of $1 \times 1\,\text{mm}^2$ was placed in the middle of the NCD layer (figure 1(a)) and surrounded by the non-patterned NCD planar layer. Below the PhC, a 280 nm-thick non-structured NCD layer remained (figure 1(b)). Finally, the residual nickel mask was removed by performing wet etching in nitro-hydrochloric acid for 5 min.

2.2. *Angle-resolved photoluminescence (PL) measurements*

PL measurements were carried out under continuous wave excitation of $50\,\text{W cm}^{-2}$ at 325 nm (along the normal to the sample) provided by a HeCd laser (Kimmon) with a plasma filter. An excitation laser beam with a diameter of $\sim 500\,\mu$m was focused on the PhC structure placed in the middle of the sample (figure 2(a)). The emitted light propagating in the Γ–X crystal direction and diffracted by the PhC was detected by an optical fiber bundle (3.2 mm in diameter, NA = 0.22) placed into a rotational holder at 23 mm distance from the sample. By mounting a circular slit (1 mm in diameter) at the input of the fiber, we obtained an angular resolution of $\sim 4^\circ$. In order to achieve angle-resolved far-field radiation measurements with no overlap between two adjacent angular windows, the optical fiber was rotated around the sample by varying the angle α in steps of 5°. The output of the optical fiber was coupled to a spectrometer equipped with a CCD camera (Andor).

2.3. *Transmission and reflection measurements*

As a light source, a broadband halogen lamp was used while the detection was performed using an optical fiber mounted with a beam coupler (5 mm in diameter) at the input, and

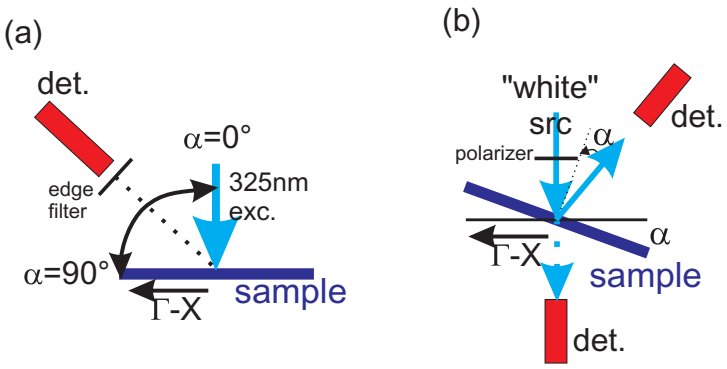

Figure 2. Sketch of the experimental setup of (a) angle-resolved PL and (b) transmission/reflection measurements.

connected to a spectrometer with an intensified CCD camera (Andor) at the output. Randomly polarized light from the source was focused on the sample through a polarizer, enabling us to carry out measurements with TE (electric field perpendicular to the plane of incidence) and TM (magnetic field perpendicular to the plane of incidence) polarized incident light. A light beam with negligible divergence (angular spread lower than 1°) and diameter around 1 mm was obtained using a pinhole and a series of lenses. The sample was rotated by the angle α around the axis parallel to the Γ–X crystal direction, allowing us to measure transmission/reflection spectra as a function of the incidence angle with a step of 2° (figure 2(b)). As a result, the component of the incident wavevector parallel to the sample plane always lay in the Γ–X direction.

In all measurements, we carefully checked the position of the fiber so that it was always facing towards the center of the excitation spot. All the presented spectra were measured at room temperature and corrected for the spectral response of the detection system.

3. Types of waveguide modes and the principle of light extraction

In this section, we describe how the waveguide modes of the smooth planar layer are affected by the introduction of a shallow PhC at the top of the layer. We apply effective index theory to describe our system and substitute the PhC part of the layer with a homogeneous medium having effective refractive index $n_{\mathrm{eff}} = 1.6$ as computed by considering the dimensions of the PhC. Thus, the PhC acts as a superstrate layer above the NCD core layer ($n_{\mathrm{NCD}} \sim 2.41$), which is positioned at the quartz substrate ($n_{\mathrm{s}} \sim 1.46$). A sketch of such a waveguiding structure is shown in figure 3(a).

Radiation of the light source can couple only to those states of field that are allowed by boundary conditions. These states, the so-called modes of the waveguide, are characterized by the in-plane wavevector $\mathbf{k}_{\parallel} = |\mathbf{k}| \sin\theta$, θ being an angle of mode propagation within the core, and the mode frequency ω, which are related through the dispersion relation (photonic band diagram) $\omega(\mathbf{k}_{\parallel})$ of the waveguide. Figure 3(b) shows a photonic band diagram of the structure depicted in figure 3(a). Based on the field profile of the mode within the waveguide, modes can be divided into guided modes, substrate, superstrate and radiation modes.

The field profile of radiation modes is extended to air and the substrate/superstrate. In the band diagram, radiation modes form a continuum of states above the air lightline $\omega = c|\mathbf{k}_{\parallel}|$ (red

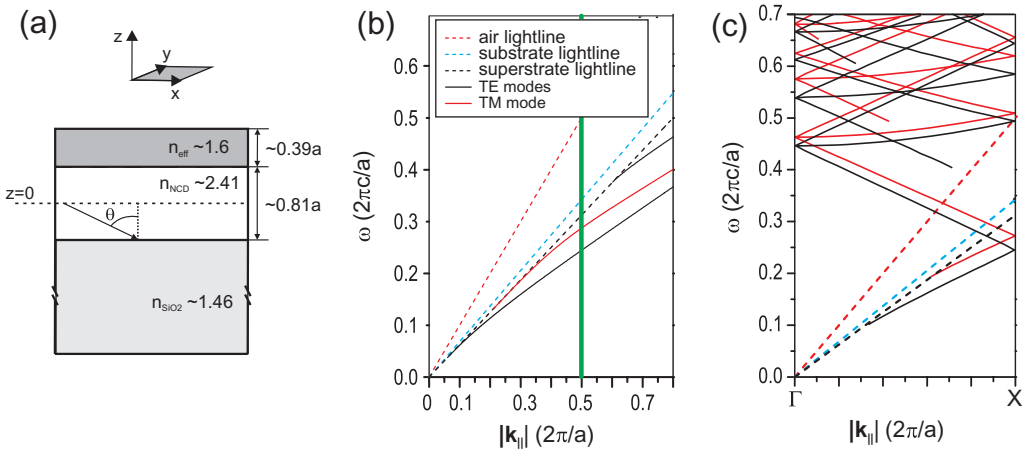

Figure 3. (a) Cross-section of our waveguide structure in the case where the effective index medium is considered instead of the PhC. Heights of the layers are expressed with respect to the lattice constant $a = 350\,\text{nm}$. (b) Photonic band diagram of the fundamental TE and TM modes, and the higher-order TE mode for a plane waveguide shown in (a). The straight vertical green line denotes the edge of the irreducible BZ in the Γ–X crystal direction of the square lattice. (c) Photonic band diagram of the PhC with a square lattice with lattice constant a in the *weak PhC* regime. Red, blue and black dashed lines represent the air, substrate and superstrate lightlines, respectively.

dashed line in figure 3), and only these modes can be detected by the far-field measurements of PL from a smooth planar layer.

Substrate modes can radiate to the substrate but due to the total reflection at the diamond–superstrate interface, they do not propagate into air. These modes lie between the air and substrate lightline $\omega = c|\mathbf{k}_\parallel|/n_s$ (blue dashed line in figure 3). Superstrate modes are in the photonic band diagram located between the substrate and superstrate lightline $\omega = c|\mathbf{k}_\parallel|/n_{\text{eff}}$ (black dashed line in figure 3).

Finally, the modes whose field profile is localized within the core and evanescent in air and the substrate/superstrate, are called the guided modes. They are characterized by an in-plane wavevector $\mathbf{k}_{\parallel\mathbf{m}}$, where m is a mode number that identifies the energy profile within the core. In the band diagram, these modes form discrete bands under the superstrate lightline.

Introducing either weakly or strongly coupled PhC into the planar layer brings the periodicity in the refractive index, which allows one to express guided modes in the form of Bloch modes, and the fundamental guided modes $\mathbf{k}_{\parallel\mathbf{m}}$ are now coupled to other harmonics $\mathbf{k}_{\parallel\mathbf{m}} + p\mathbf{G}$ by the reciprocal vector $|\mathbf{G}| = 2\pi/a$ [13], where p is an integer identifying the harmonic. Those harmonics which satisfy a diffraction condition $|\mathbf{k}_{\parallel\mathbf{m}} + p\mathbf{G}| < 2\pi/\lambda$ are diffracted by the PhC into the surrounding air during their propagation in the core. These are the so-called leaky modes[9], or guided resonances [18], which couple with the radiation modes inside the air lightcone.

[9] The term 'leaky modes' in the case of the planar uncorrugated waveguide can correspond to extended modes at the boundary of the lightcone that are traveling parallel to the boundary.

As for a PhC, the photonic band diagram is expressed along the high-symmetry directions of the irreducible Brillouin zone (BZ) of the crystal lattice and can be computed by several computational methods from the characteristics of the structure. However, the qualitative picture of the band diagram of a shallow PhC at the top of the waveguiding layer can be derived from dispersion relations of the planar uncorrugated waveguide by folding the bands at the edges of the irreducible BZ [9]—the edge of the BZ in the Γ–X direction of the square lattice is in figure 3(b) denoted by the green vertical line.

The folded photonic band diagram in the Γ–X crystal direction of a square lattice of the planar waveguide (figure 3(c)) was computed by the finite-difference time-domain method [24]. A light source positioned in the plane $z = 0$ and having either an electric or a magnetic field parallel to the layer was used in order to excite TE (black curves) or TM modes (red curves). TM modes have the same shape of dispersion curve as TE modes but slightly shifted towards higher frequencies. One can clearly see folding of the first-order TE and TM modes at the edge of the BZ, which leads to the fact that discrete bands—leaky modes—appear above the air lightline. Other bands arising from folding of higher-order TE and TM modes start at higher frequencies. As they occur above the air lightline, they can be accessible by the far-field PL measurements. A qualitatively very similar band diagram can be computed for the Γ–M crystal direction, leading to a similar physical phenomenon (coupling to leaky modes) as in the Γ–X direction. Photonic properties in this direction are not studied here; however, it should be noted that the extraction efficiency in this direction would be dependent on the leaky-mode band structure and consequent spectral overlap with the emission of the diamond, along with the modal coupling efficiencies.

The diffraction efficiency of the PhC depends strongly on the spatial overlap of the guided mode with the PhC [9]. Therefore, guided modes that penetrate into the PhC are well extracted, whereas modes that are strongly confined in the core are diffracted only poorly. Also the lattice spatial symmetry affects the extraction properties of the PhC. It was shown that the lattice with square symmetry allows high extraction efficiency in a larger wavelength and angular bandwidth compared to the triangular lattice, which mostly extracts in the direction normal to the sample plane [15]. In addition to guided modes, the substrate modes can also interact with the PhC and thus be diffracted. However, most of these modes have low field overlap with the PhC and are usually lost in the substrate.

4. Experimental results and discussion

4.1. Enhancement of PL extraction

Angular far-field PL radiation patterns for both the planar 417 nm-thick NCD layer and the PhC in the Γ–X direction are shown in figures 4(a) and (b), respectively (note the identical intensity scale). The PL spectra of the planar NCD layer (figure 4(a)) exhibit a relatively flat profile of emission intensities across the whole visible region with two broad PL maxima for each detection angle α due to the F–P resonances of radiation modes between the diamond–silica and the diamond–air interface (figures 4(c) and (d)—red line). The reason for the very poor light extraction is that most of the light emitted from the diamond defects in the uncorrugated NCD layer is coupled either to guided or substrate modes and only $\sim$4% of the overall light power reaches air.

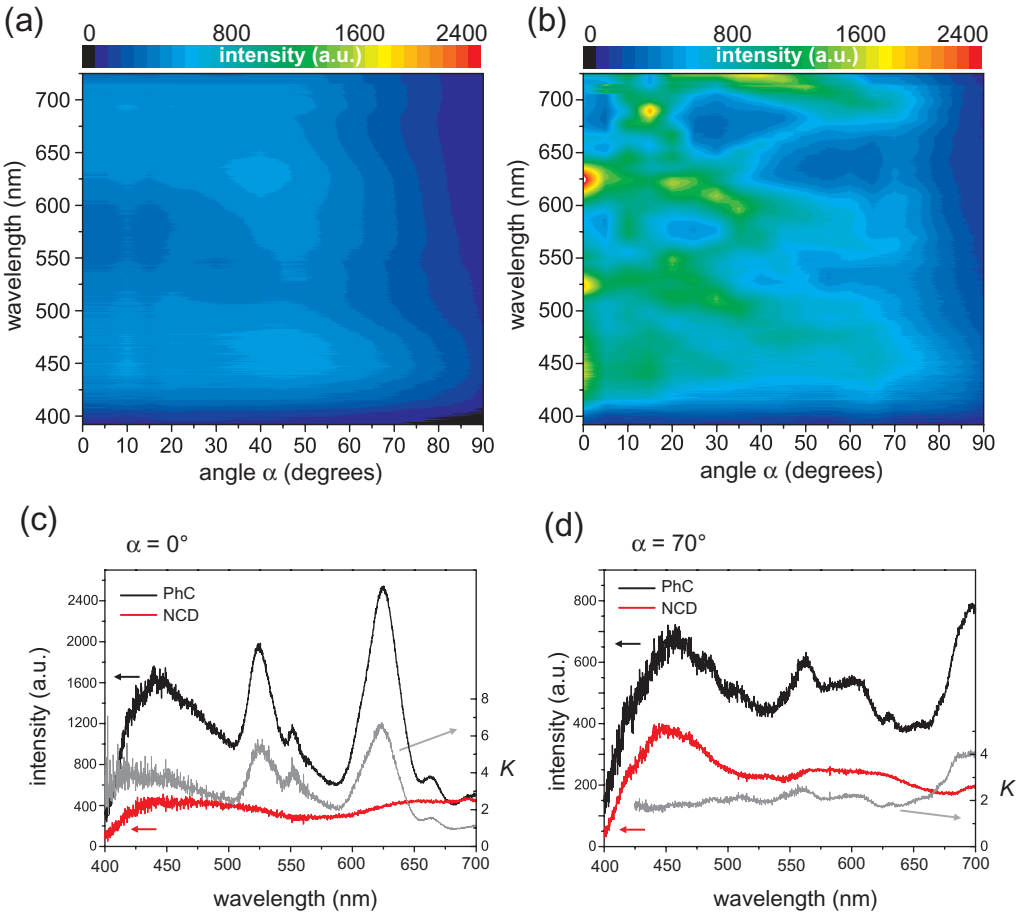

Figure 4. Angular far-field patterns of PL emitted in the Γ–X direction from (a) the planar 417 nm-thick NCD layer itself and (b) the NCD layer with PhC structure. Profile graphs of PL taken from (a) and (b) for the detection angle $\alpha = 0^\circ$ (c) and $\alpha = 70^\circ$ (d), and the relevant ratio K of the PL intensities of the PhC structure and the uncorrugated NCD layer.

On the other hand, PL spectra of the NCD layer with the PhC strongly dependent on wavelength and detection angle, exhibit a distinct structure composed of several peaks for each detection angle superimposed on a broad F–P background (figures 4(c) and (d)—black line). We can assume that the intensity I_{PhC} detected from the PhC is related to the PL intensity from the uncorrugated NCD layer I_{NCD} via the relation

$$I_{\mathrm{PhC}}(\lambda, \alpha) = K(\lambda, \alpha) I_{\mathrm{NCD}}(\lambda, \alpha), \tag{1}$$

where $K(\lambda, \alpha)$ is a factor depending on the parameters of the PhC and consisting of several contributions, which will be discussed further. It also defines the enhancement of PL extraction efficiency from the PhC compared to the uncorrugated layer. Maximal, up to six-fold, enhancement was detected for the direction normal to the sample ($\alpha = 0^\circ$, figure 4(c)), which occurs due to the degeneracy of leaky modes at the Γ-point. Even though most of the extracted light power is focused into the directions close to the sample normal, more than two-fold enhancement over the whole spectral region is still present for larger detection angles as depicted

for $\alpha = 70^\circ$ in figure 4(d). The PL enhancement K clearly arises from the presence of the PhC and may comprise several effects that will be discussed later.

The origin of the PL from the NCD layer is presumably due to dislocations and other defects that are introduced within grains [25] (either in their volume or at their surface) of which the layer is composed. Therefore, simple variations in geometry themselves may play a role in the enhancement of extraction efficiency. First, an active surface area $S_0 = 1\,\mathrm{mm}^2$ of the NCD planar layer is increased by its nanopatterning to the value $S = S_0 + \Delta S$, where $\Delta S \sim 0.79\,\mathrm{mm}^2$, which leads to an increased amount of light-emitting centers positioned at the surface of the pillars emitting directly to the surrounding air. We shall, in crude approximation, assume that the changes in surface area and number of surface centers are related to each other linearly. Next, we will consider only the following three main processes to occur. Part of the light emitted from the surface defects goes directly to the detector and another part gets diffracted on surrounding pillars either into air or into the underlying NCD layer. We shall assume all three processes have comparable weight due to their randomness. Therefore, only two thirds of the emitted light will contribute to the enhancement due to increased active surface. The remaining one third will penetrate into the layer.

Secondly, when forming nanopillars on the layer, part of the material was taken away, decreasing the active volume of the PhC structure with the underlying layer from a value V_0 of the uncorrugated layer to a smaller value V. Considering our dimensions of the PhC structure (figure 1(b)), we obtain a ratio $\Delta V/V_0 \sim -0.23$, where $\Delta V = V - V_0$.

Thirdly, the coupling of the excitation laser light into the layer may be enhanced by the presence of the PhC [26]. The incident 325 nm light becomes diffracted on the periodically ordered nanopillars and thus excites a larger amount of the volume of the material than is the actual volume of the PhC structure. Its contribution can be expressed with the factor $C_{\mathrm{exc}} \sim 1.3$, whose value was estimated from a ray optics model of diffraction on the grating. Taken together, we can express the parameter K as

$$K(\lambda, \alpha) = A_{\mathrm{PhC}}(\lambda, \alpha) C_{\mathrm{exc}} [1 + \Delta V/V_0]^{\frac{2}{3}} [1 + \Delta S/S_0] \sim 1.2\, A_{\mathrm{PhC}}, \tag{2}$$

where A_{PhC} is a parameter that characterizes the contribution of the PhC effect to the overall enhancement. This relation assumes that the probability of emission from the defect positioned at the surface of the layer and from the defect located inside is similar. This is reasonable because the origin of these defects is believed to be identical, both being introduced during the preparation process [25]. If we consider the experimental value $K \in (2\text{–}6)$, we get $A_{\mathrm{PhC}} \in (1.7\text{–}5)$, which produces a rather high enhancement of extraction efficiency due to the influence of PhC on the guided modes as described in section 3. The remaining effects cause merely an increased background in PhC PL spectra.

4.2. Photonic band diagram analysis

Leaky modes manifest themselves as relatively narrow minima in the transmission spectra superimposed on slowly varying F–P resonances [19]. The depth of these minima reflects the efficiency of the light coupling into the structure, and at the same time it indicates how effectively the light generated inside the structure will interact with the PhC and be outcoupled from the structure. On the other hand, in reflection spectra, Fano-like shaped maxima occur at the same spectral positions. This effect is demonstrated for our PhC sample in figures 5(a) and (b) for TE and TM polarized light incident at the angle $\alpha = 20^\circ$, respectively. From a comparison

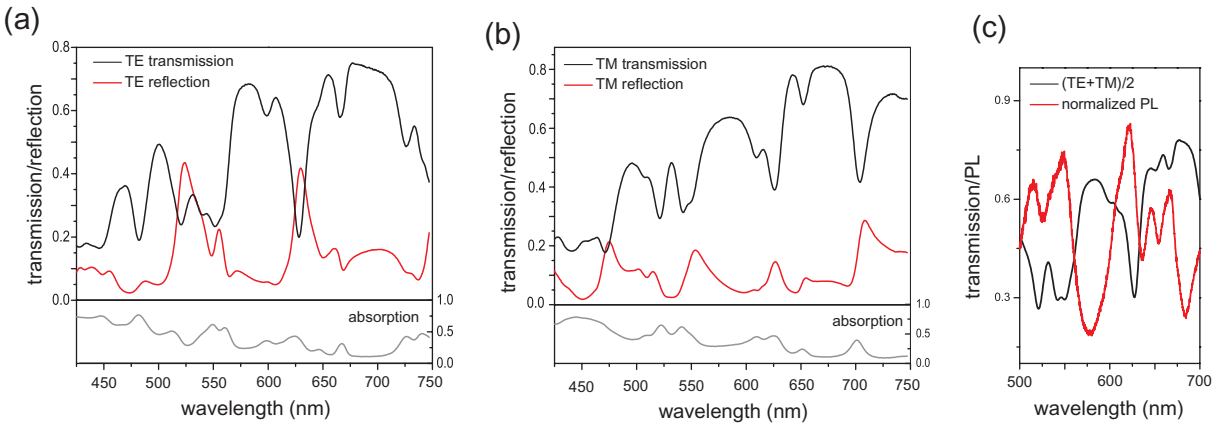

Figure 5. Transmission, reflection and absorption (1 − transmission − reflection) spectra from the PhC obtained with (a) TE and (b) TM polarized light incident at $\alpha = 20^\circ$ along the Γ–X symmetry direction. (c) Comparison of normalized PL spectra and averaged TE and TM transmission spectra for $\alpha = 20^\circ$ within the narrow spectral region.

of these two figures, we see that each light polarization excites different modes based on their symmetry. The gray curve depicts absorption given by the relation (1 − transmission − reflection) and it slowly rises towards the lower wavelengths, suggesting that the NCD layer is more absorbing in the blue spectral region. Furthermore, peaks in absorption being at the spectrally same position as leaky modes suggests that some part of the incident coupled light remains in the structure without being outcoupled forward or backward.

Direct comparison of the normalized PL emission spectra with the averaged TE and TM transmission curves [(TE + TM)/2] of the PhC for $\alpha = 20^\circ$ (figure 5(c)) shows that the PL maxima occur at nearly the same spectral position as transmission minima and so at the same position as leaky modes. It indicates that the light outcoupling from the PhC occurs via the same radiative channel, leaky modes, as the coupling into the structure.

A PhC band diagram (figure 6(a)), in the angle–wavelength representation, within the investigated spectral region in the Γ–X symmetry direction was derived from the PL spectra shown in figure 4(b) by normalizing to the maximum at each angle and by correcting for the source spectrum profile obtained from the uncorrugated layer. Moreover, it is overlaid with the computed photonic band diagram derived from TE dispersion relations shown in figure 3(c) by converting its axes into the angle–wavelength representation and having the bands that occur in the measured band diagram as the most intense ones, highlighted by black lines. Despite the simple approximation of the effective refractive index used in the calculation in order to describe the real structure, the shape of the measured bands is very well reproduced in the simulation. The slight difference in the spectral position of computed and measured bands was compensated by shifting the simulated bands to match the spectral position of measured ones. TM modes are not shown in order to keep the diagram lucid; however, they would appear shifted towards lower wavelengths with the same dispersion behavior as TE bands.

The photonic band diagram derived from PL measurements is in good agreement with a photonic band diagram (figure 6(b)) derived from unpolarized transmission spectra measured for angles 0°–26° by normalizing on the absorption profile of the NCD.

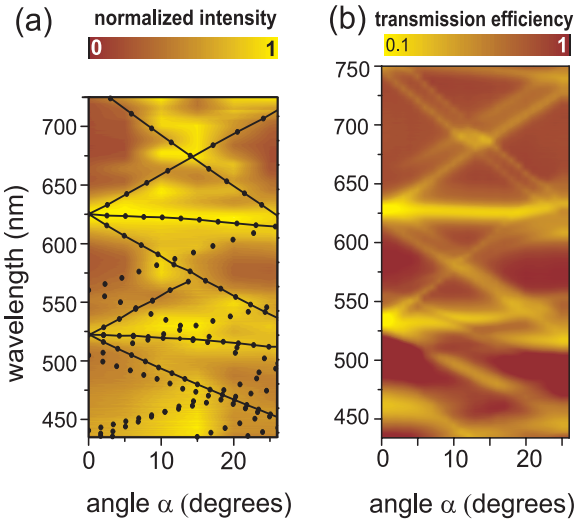

Figure 6. Photonic band diagram of the PhC in the α–λ representation: (a) derived from the PL measurements shown in figure 4(b) and overlaid with the calculated TE band diagram shown in figure 3(c); and (b) derived from transmission spectra of the PhC.

Relatively narrow photonic bands of leaky modes starting at ∼625 nm and ∼530 nm can be identified in both the diagrams. For the wavelengths below 500 nm, PL peaks or similarly transmission minima lose their fine structure and become broader but still, even for them, PL extraction remains enhanced compared with PL of the smooth layer. This suggests that the broad band starting at ∼460 nm arises from overlapping of many leaky modes located close together in the band diagram, which is also supported by the results of photonic band diagram simulation in which densely positioned modes are present in the blue spectral region.

In the spectral region of 630–750 nm, bands closely spaced and parallel to each other can be seen, which arises due to TE–TM splitting. Moreover, it is worth noting that diffraction efficiency is very high in areas where the crossing between two bands occurs (compare figures 4(b) and 6(b)).

We can thus summarize that the agreement between theory and experiment signifies that we still operate in *the weak PhC* regime even though the PhC structure is relatively deeply etched into the NCD layer and that the extraction of the light emitted inside the NCD layer is enhanced mainly due to the light being coupled to leaky modes.

5. Conclusions

In conclusion, we demonstrated up to six-fold enhancement of extraction of intrinsic PL from an NCD layer by nanopatterning its top part into a PhC. We tuned the design of the PhC so that the enhancement was high within a broad spectral region. We showed that the physics underlying this effect consists in the fact that the PhC structure, on the one hand, serves as a coupler of the excitation laser radiation into the structure allowing efficient excitation of diamond defects and, more importantly, acts as a Bragg diffraction grating, which diffracts light emitted from the diamond defects into air. The complementarity between the angular far-field

PL and transmission measurements of the PhC was demonstrated, and the photonic diagram extracted from both of these measurements is in qualitative agreement with the simulated one. The results of this study might be useful for applications in the field of optics and optoelectronics while tuning and increasing the emission properties of diamond LEDs or can be applied in the construction of light couplers to NCD waveguides.

Acknowledgments

We thank T Ostatnický for fruitful discussions and K Hruška and Z Poláčková for technical support. This work was supported by the Centrum MŠMT (grant number LC510), GAAV (grant number IAA101120804), GAAV (grant number KJB100100903), GAUK (grant number 73910 and SVV-2011-263306), AVCR (grant number KAN400100701), the Institutional Research Plan (grant number AV0Z 10100521) and the J E Purkyně Fellowship.

References

[1] Zaitsev A M 2001 *Optical Properties of Diamond: A Data Handbook* (Berlin: Springer)
[2] Pan L S (ed) 1995 *Diamond: Electronic Properties and Applications* (New York: Kluwer Academic)
[3] Field J E (ed) 1992 *Properties of Natural and Synthetic Diamond* (New York: Academic)
[4] Koizumi S, Watanabe K, Hasegawa M and Kanda H 2001 Ultraviolet emission from a diamond pn junction *Science* **292** 1899
[5] Takeuchi D, Makino T, Kato H, Ogura M, Tokuda N, Oyama K, Matsumoto T, Hirabayashi I, Okushi H and Yamasaki S 2010 Electron emission from a diamond (111) p–i–n(+) junction diode with negative electron affinity during room temperature operation *Appl. Phys. Express* **3** 041301
[6] Gruber A, Dräbenstedt A, Tietz C, Fleury L, Wrachtrup J and von Borczyskowski C 1997 Scanning confocal optical microscopy and magnetic resonance on single defect centers *Science* **276** 2012–4
[7] Wierer J J *et al* 2001 High-power AlGaInN flip-chip light-emitting diodes *Appl. Phys. Lett.* **78** 3379
[8] Fujii T, Gao Y, Sharma R, Hu E L, DenBaars S P and Nakamura S 2004 Increase in the extraction efficiency of GaN-based light-emitting diodes via surface roughening *Appl. Phys. Lett.* **84** 855–7
[9] Wiesmann Ch, Bergenek K and Schwarz U T 2009 Photonic crystal LEDs—designing light extraction *Laser Photonics Rev.* **3** 262–86
[10] Matioli E and Weisbuch C 2010 Impact of photonic crystals on LED light extraction efficiency: approaches and limits to vertical structure designs *J. Phys. D: Appl. Phys.* **43** 354005
[11] Fan S, Villeneuve P R, Joannopoulos J D and Schubert E F 1997 High extraction efficiency of spontaneous emission from slabs of photonic crystals *Phys. Rev. Lett.* **78** 3294–7
[12] Fujita M, Takahashi S, Tanaka Y, Asano T and Noda S 2005 Simultaneous inhibition and redistribution of spontaneous light emission in photonic crystals *Science* **308** 1296–8
[13] Wierer J J, David A and Megens M M 2009 III-nitride photonic-crystal light-emitting diodes with high extraction efficiency *Nat. Photonics* **3** 163–9
[14] Bergenek K, Wiesmann Ch, Wirth R, O'Faolain L, Linder N, Streubel K and Krauss T F 2008 Enhanced light extraction efficiency from AlGaInP thin-film light-emitting diodes with photonic crystals *Appl. Phys. Lett.* **93** 041105
[15] Ganesh N, Block I D, Mathias P C, Zhang W, Chow E, Malyarchuk V and Cunningham B T 2008 Leaky-mode assisted fluorescence extraction: application to fluorescence enhancement biosensors *Opt. Express* **16** 21626
[16] Boroditsky M, Vrijen R, Krauss T F, Coccioli R, Bhat R and Yablonovitch E 1999 Spontaneous emission extraction and Purcell enhancement from thin-film 2-D photonic crystals *J. Lightwave Technol.* **17** 2096–112

[17] Astratov V N, Whittaker D M, Culshaw I S, Stevenson R M, Skolnick M S, Krauss T F and De La Rue R M 1999 Photonic band-structure effects in the reflectivity of periodically patterned waveguides *Phys. Rev.* B **60** 16255–8

[18] Fan S and Joannopoulos J D 2002 Analysis of guided resonances in photonic crystal slabs *Phys. Rev.* B **65** 235112

[19] Ganesh N, Zhang W, Mathias P C, Chow E, Soares J A N T, Malyarchuk V, Smith A D and Cunningham B T 2007 Enhanced fluorescence emission from quantum dots on a photonic crystal surface *Nat. Nanotechnol.* **2** 515–620

[20] Ondič L, Dohnalová K, Ledinský M, Kromka A, Babchenko O and Rezek B 2011 Effective extraction of photoluminescence from a diamond layer with a photonic crystal *ACS Nano* **5** 346–50

[21] Kromka A, Rezek B, Remes Z, Michalka M, Ledinsky M, Zemek J, Potmesil J and Vanecek M 2008 Formation of continuous nanocrystalline diamond layers on glass and silicon at low temperatures *Chem. Vapor Depos.* **14** 181–6

[22] Dzurnak B, Trojanek F, Preclikova J, Kromka A, Rezek B and Maly P 2009 Subgap photoluminescence spectroscopy of nanocrystalline diamond films *Diam. Relat. Mater.* **18** 776–8

[23] David A, Benisty H and Weisbuch C 2007 Optimization of light-diffracting photonic-crystals for high extraction efficiency LEDs *J. Disp. Technol.* **3** 133–48

[24] Oskooi A F, Roundy D, Ibanescu M, Bermel P, Joannopoulos J D and Johnson S G 2010 MEEP: a flexible free-software package for electromagnetic simulations by the FDTD method *Comput. Phys. Commun.* **181** 687–702

[25] Philip J, Hessa P, Butler J E, Chattopadhyay S, Chen K H and Chen L C 2003 Elastic, mechanical and thermal properties of nanocrystalline diamond films *J. Appl. Phys.* **93** 2164

[26] Erchak A A, Ripin D J, Fan S, Rakich P, Joannopoulos J D, Ippen E P, Petrich G S and Kolodziejski L A 2001 Enhanced coupling to vertical radiation using a two-dimensional photonic crystal in a semiconductor light-emitting diode *Appl. Phys. Lett.* **78** 563